NONDESTRUCTIVE INSPECTION OF HIGH PERFORMANCE CERAMICS

R. H. Brockelman
Army Materials and Mechanics Research Center
Watertown, Massachusetts 02172

ABSTRACT

Two ceramic materials, a hot-pressed silicon nitride and a siliconized silicon carbide, were manufactured with seeded particulates to evaluate the effectiveness of existing nondestructive test practices at AMMRC for defect detection in ceramics and to evaluate the effect of inclusions upon material strength. The types of seeded defects were of greater and lower density relative to the matrix materials and ranged in size from approximately 0.1 mm to 0.6 mm. The nondestructive methods used in the investigation were ultrasonics, radiography, eddy current and penetrant. Bend bar specimens were cut from the seeded regions of the billets and tested at 25°C, 1093°C and 1371°C. Fracture origins were examined by optical and electron microscopy and by microprobe to correlate the nature of the fracture initiating defects with the nondestructively detected defects. This permitted a ranking of defect detection sensitivity and defect effect upon strength.

SUMMARY

Two billets approximately 15 centimeters square of each matrix material were prepared with seeded inclusion particles from standard production powder mixes. The inclusion defects selected for incorporation into the hot pressed silicon nitride (HPSN) were graphite (C), iron (Fe), silicon (S) and tungsten carbide (WC) particles. The same types of particles, with the exception of tungsten carbide, were seeded into the silicon carbide (SiC) billets.

Maps of the seeded inclusion locations and corresponding ultrasonic pulse-echo C-scan recordings of the billets following surface machining are shown in Figs. 1-4. The nominal sizes of fine, medium, and course correspond to mean particle diameters of approximately 125, 250, and 635 microns. The ultrasonic test reveals the presence of many defects in the billets that are not listed on the seed location maps. Fig. 5 shows C-scan recordings of the variation in ultrasonic energy loss through the surface machined SiC billets. White areas represent a 3db or 2 times loss of energy compared to dark areas. Point by point ultrasonic velocity measurements in the billets showed an average longitudinal wave velocity for the HPSN billets of 1.12 cm/μsec with a variation of less than 1 percent between measurements. The SiC billets had variations up to 3 percent with an average of 1.21 cm/μsec.

Figure 6 presents variations in eddy current response of a SiC billet. The numerical values are only relative showing variation in resistivity with a single billet. Each billet was examined by liquid penetrant for surface cracks, porosity and edge laminations. A map of liquid penetrant indications in a SiC billet is shown in Fig. 7. The HPSN billets were free of indications. Positive prints of radiographs of the billets are shown in Fig. 9. All sizes of the tungsten carbide and iron contaminants in the HPSN billets are visible. The fine and medium size silicon and graphite particles were not visible in the HPSN billets. Only the large graphite particles and a surface scab are visible in the radiograph of the SiC billet.

Figures 10 and 11 contain examples of individual C-scans of rough-cut bend bars sectioned from the billets and the subsequent microscope analyses of defects contained within the corresponding bend bars. The latter includes photomicrographs of the fracture initiating defect and a photograph of the display of the energy dispersive microprobe. The photomicrographs are oriented such that the thickness direction of the bend bar corresponds to the vertical direction of the page. The C-scans were made from both the front and back sides of the bars. In addition to the two dimensional displays of the defect positions (in plane of paper), the depth (in direction perpendicular to plane of paper) of the defects are tabulated, as determined by the method of detection. Depths are measured relative to the back surface of the bar. The following abbreviations are used in the C-scans:

F	-	Front surface view
B	-	Back surface view
DN	-	Defect number
USD	-	Depth of defect as determined by ultrasonics distance measured from back surface (B) in inches.
XRD	-	Depth of defect as determined by radiography distance measured from back surface (B) in inches.
H	-	Defect density higher than that of matrix.
L	-	Defect density lower than that of matrix.

In the listing of the defects below a C-scan figure, an arrow indicates the defect which was sought as the fracture origin (target defect). Multiple defects were present upon occasion at the same depth within the sample.

Results of bend bar testing and a ranking of defect detection sensitivity and defect effect upon strength can be found in the following Reference:

H. R. Baumgartner, R. H. Brockelman, P. M. Hanson, Development of Nondestructive Testing Techniques for High Performance Ceramics. AMMRC TR 78-11 (Army Materials and Mechanics Research Center, Jan. 1978).

ACKNOWLEDGMENT

This project was a joint effort with the Nondestructive Testing Industrial Applications Branch, at the Army Materials and Mechanics Research Center, and Norton Company, Worcester, Massachusetts, and has been accomplished as part of the U. S. Army Materials Testing Technology Program. The nondestructive evaluation of the ceramic materials was performed at AMMRC under the direction of Mr. C. H. Hastings. The Project Manager at Norton was H. R. Baumgartner.

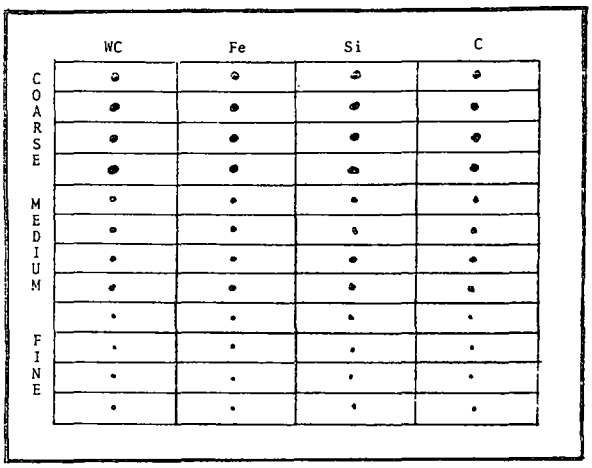

Fig. 1. Defect seeding plan for hot-pressed silicon nitride billets.

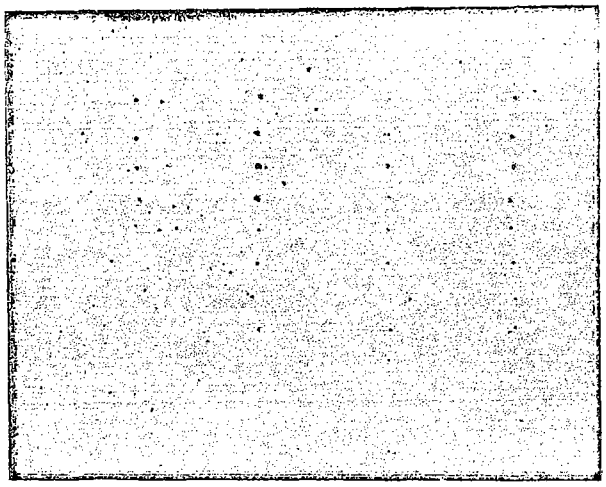

Top Billet

Bottom Billet

Fig. 2. Ultrasonic C-scan recordings at 25 MHz of defects in hot-pressed silicon nitride billets.

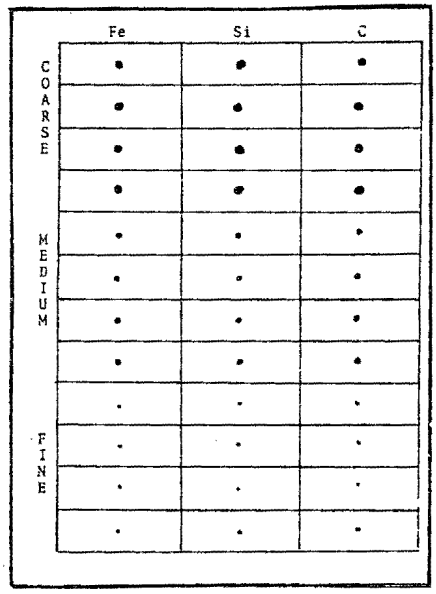

Fig. 3. Defect seeding plan for silicon carbide billet.

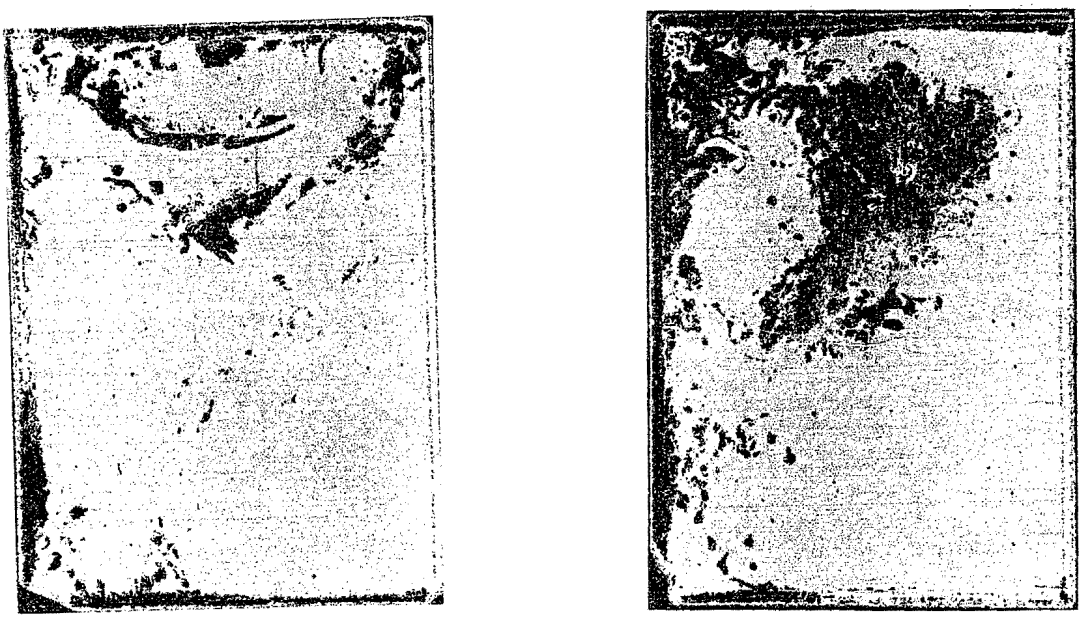

No. 1 Billet

No. 2 Billet

Fig. 4. Ultrasonic C-scan recordings at 25 MHz of defects in siliconized silicon carbide billet.

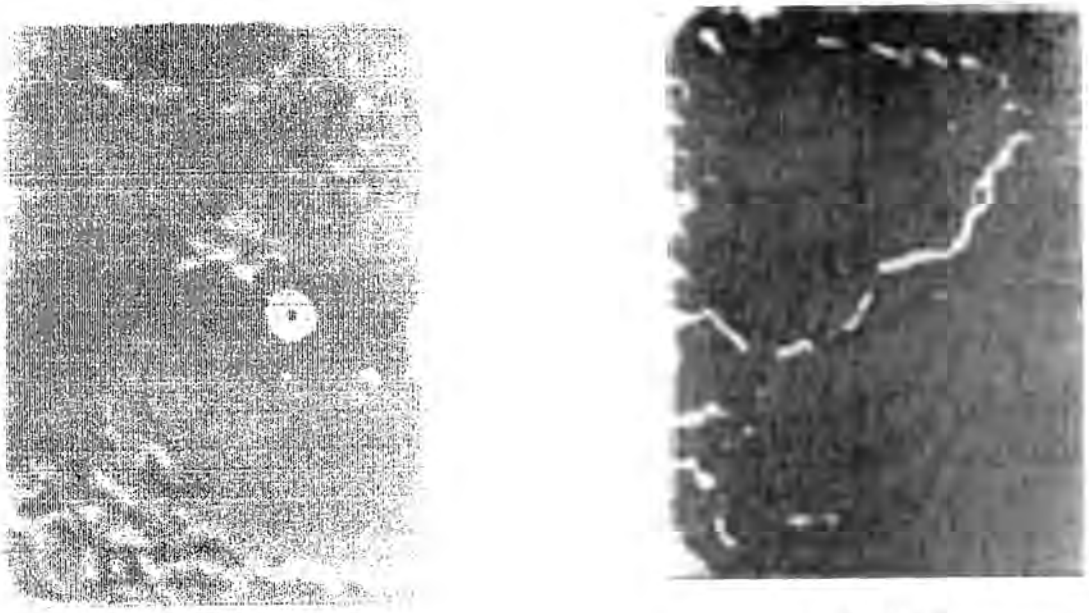

No. 1 Billet

No. 2 Billet

Fig. 5. Ultrasonic C-scan recordings at 15 MHz of attenuation changes in silicon carbide billets.

	Fe	Si	C
C	2.8	5.0	7.0
	3.0	6.0	7.6
0 X	0.2 X 3.5	2.8	8.5
	2.3	2.9	10.0 X 8.4
	1.4	9.5	7.0
	2.0	7.5	6.4
M	2.8	6.2	6.2
	5.0	6.0	5.6
	6.2	5.4	5.4
	4.9	4.9	4.6
F	3.0	3.6	4.0
	3.1	2.4	2.0

Fig. 6. Variations in eddy current response of silicon carbide No. 2 billet.

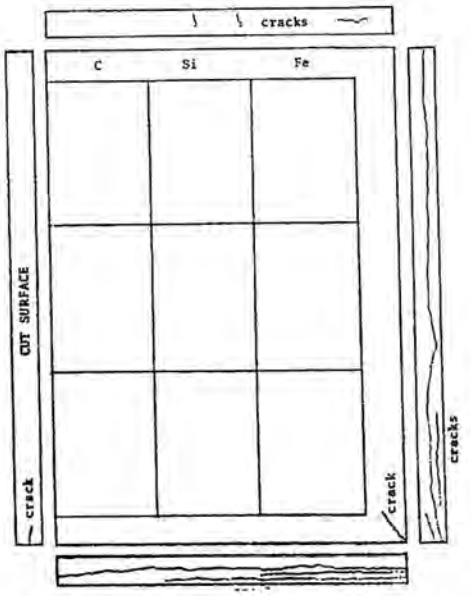

Fig. 7. Map of liquid penetrant indications of silicon carbide No. 2 billet, turned over.

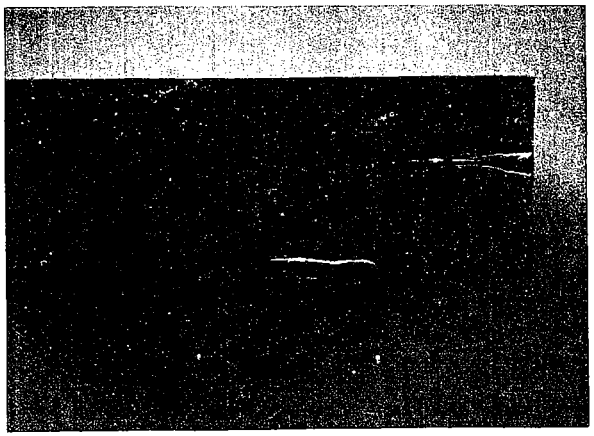

Fig. 8. Black light photograph of fluorescent penetrant indications of silicon carbide.

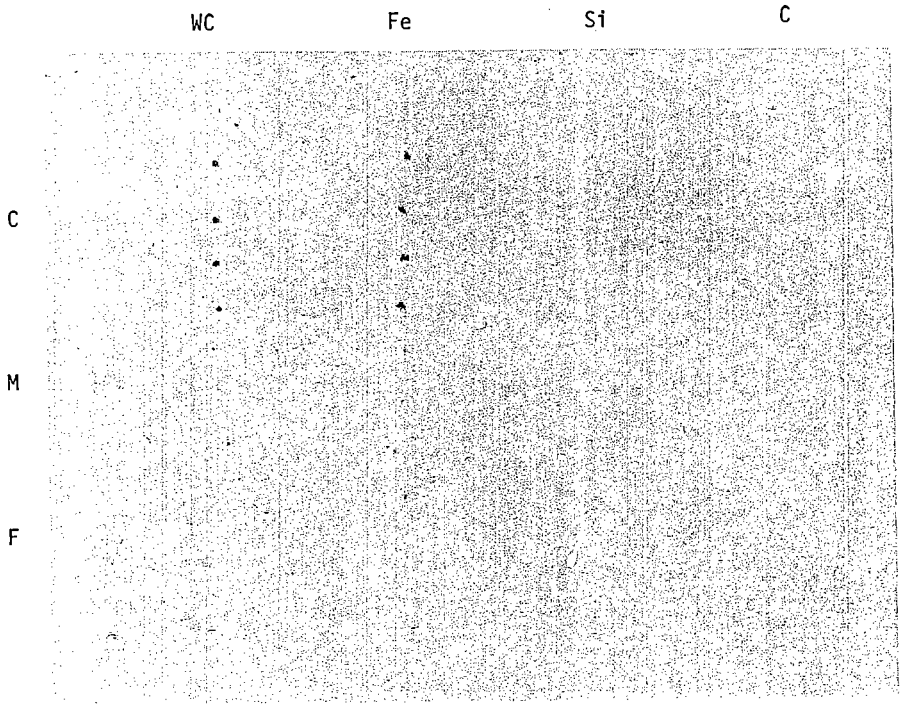

HPSN Top Billet

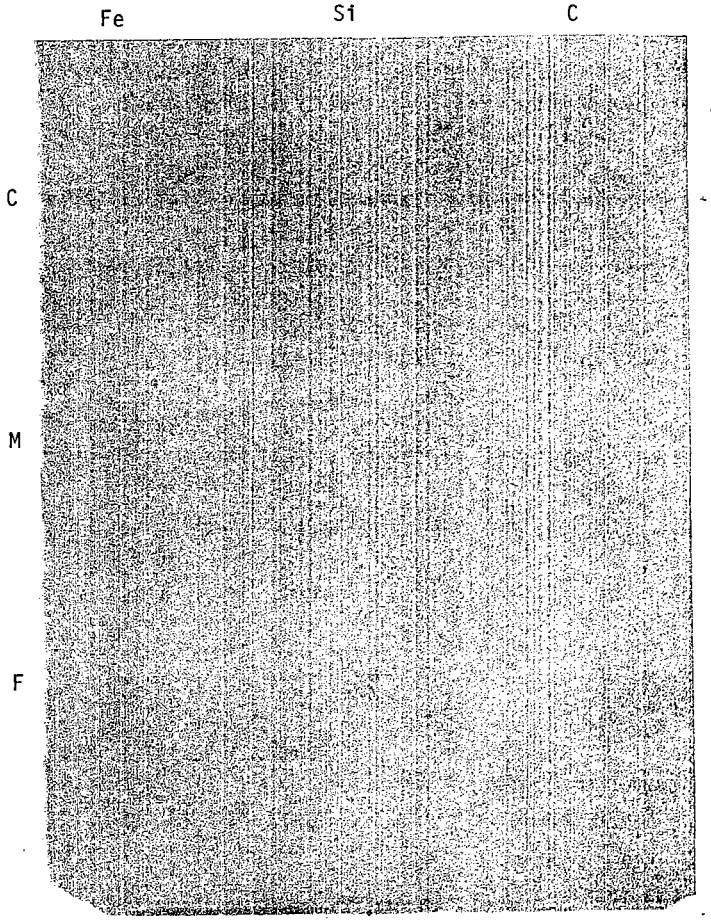

SiC No. 1 Billet

Fig. 9. Positive prints of radiographs of billets.

HPSN Bottom billet, medium size tungsten carbide inclusion, defect number (DN) 4.

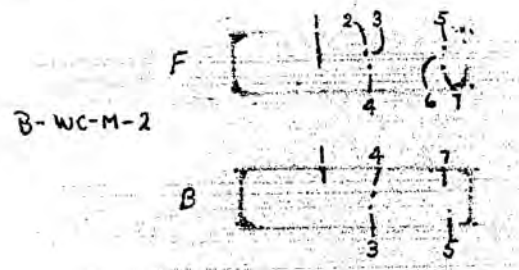

DN	USD	XRD
1	0.099	
2	0.109	
3	0.109	
→ 4	0.109	0.105 H
5	0.109	
6	0.109	
7	0.109	

HPSN Bottom billet, fine size iron inclusion, defect number (DN) 3, test temperature 1093°C.

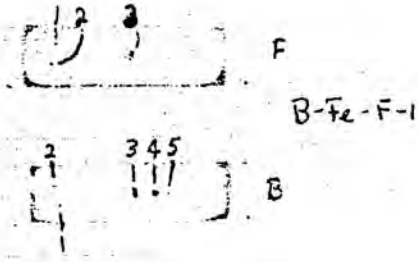

DN	USD	XRD
1	0.109	
2	0.109	
→ 3	0.109	0.105 H
4	0.118	
5	0.109	

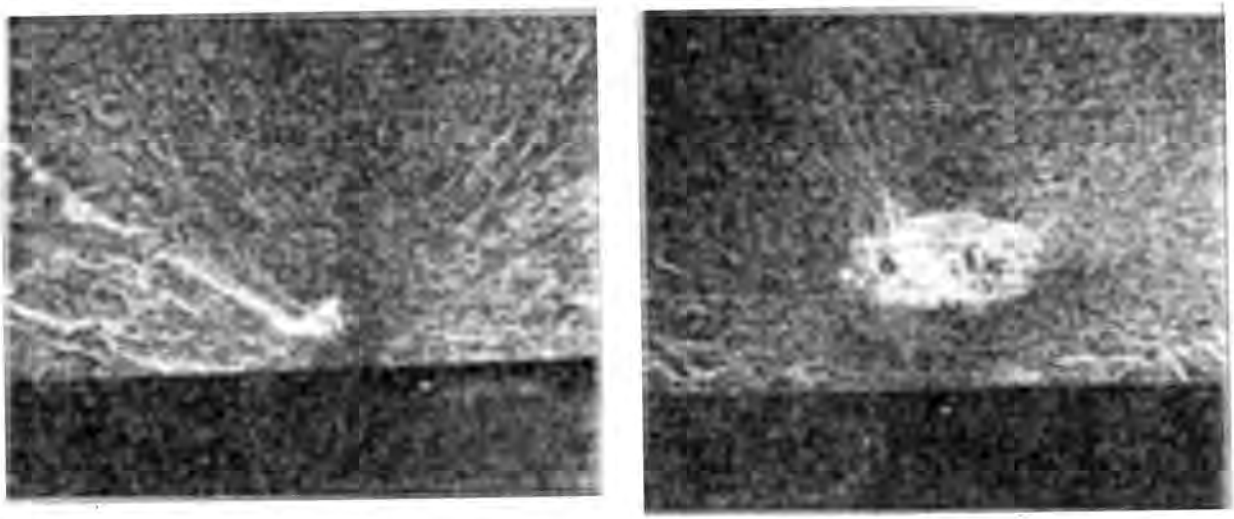

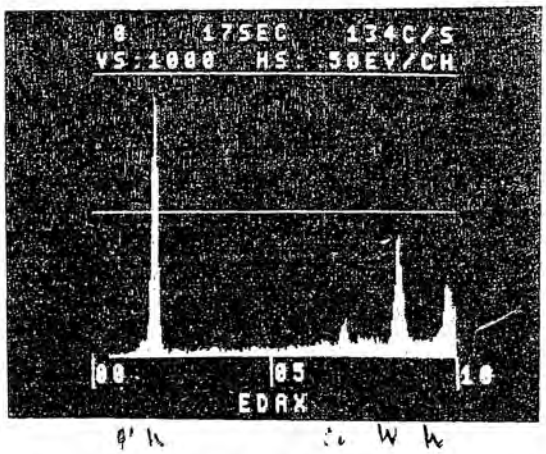

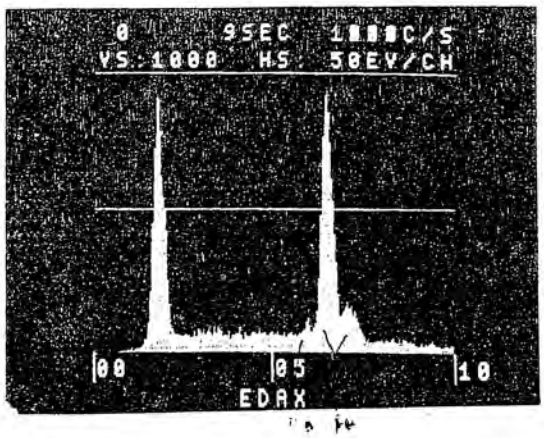

Fig. 10. C-scan (above), scanning electron microscope view of inclusion at fracture origin, 50X, (middle) and photograph of electron microprobe display (below) of hot-pressed silicon nitride bend bars.

SiC No. 1 Billet, coarse size iron inclusion, defect number (DN) 1.

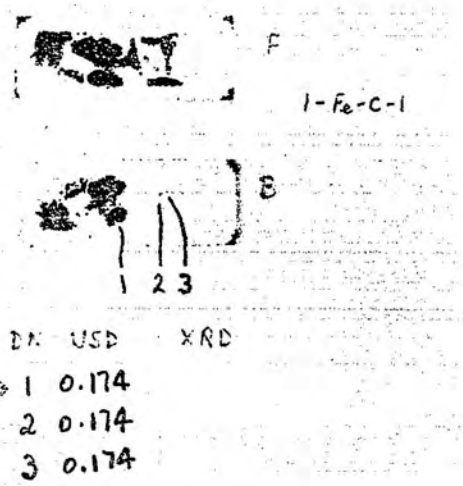

DN	USD	XRD
→ 1	0.174	
2	0.174	
3	0.174	

SiC No. 2 Billet, medium size carbon inclusion, defect number (DN) 1, test temperature 1371°C.

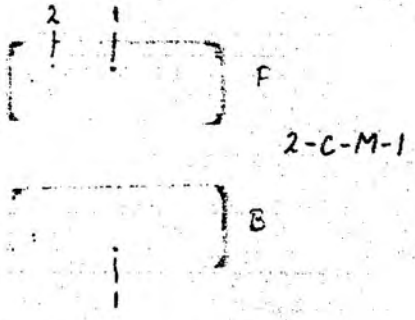

DN	USD	XRD
→ 1	0.146	
2	0.186	

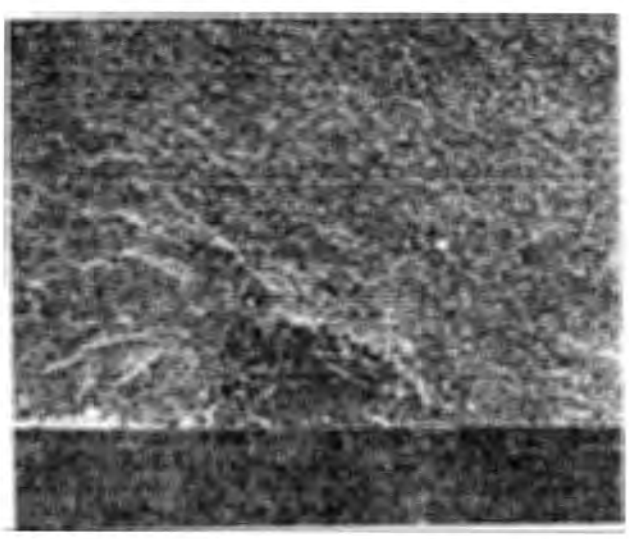

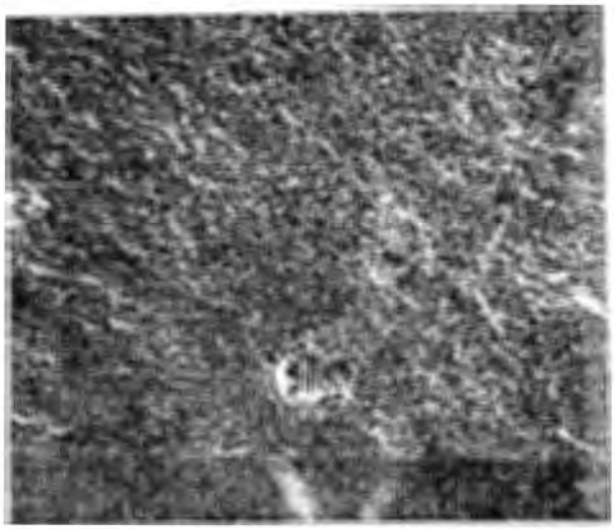

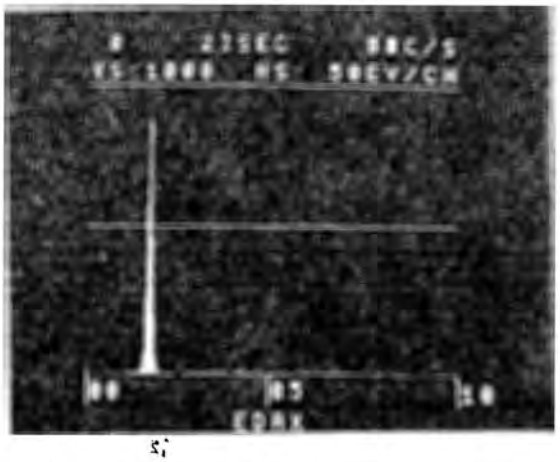

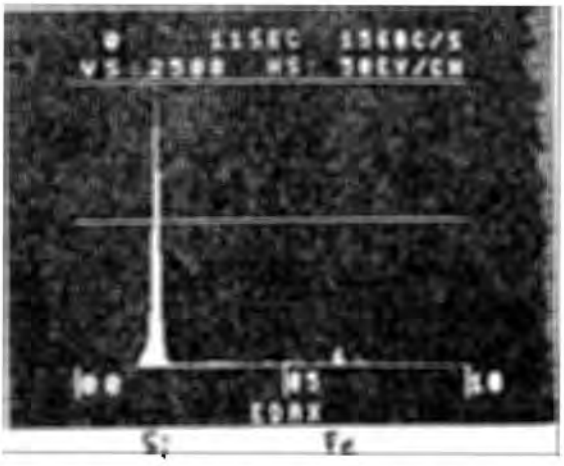

Fig. 11. C-scan (above), scanning electron microscope view of inclusion at fracture origin, 50X, (middle) and photograph of electron microprobe display (below) of silicon carbide bend bars.